ISSN (Print) 1226-1750
ISSN (Online) 2233-6656
Journal of Magnetics 25(4), 453-457 (2020) https://doi.org/10.4283/JMAG.2020.25.4.453

Effects of Scandium Doping on Structural and Magnetic Properties of Cobalt Ferrite Thin Films

Kwang Joo Kim[1], Jongho Park[1], and Jae Yun Park[2]*

[1]*Department of Physics, Konkuk University, Seoul 05029, Korea*
[2]*Department of Materials Science and Engineering, Incheon National University, Incheon 22012, Korea*

(Received 24 August 2020, Received in final form 24 November 2020, Accepted 1 December 2020)

Structural and magnetic properties of Sc-substituted cobalt ferrites were studied by X-ray diffraction, Raman spectroscopy, X-ray photoelectron spectroscopy, and vibrating-sample magnetometry. The $Sc_xCoFe_{2-x}O_4$ ($x \leq 0.3$) specimens prepared as thin films by a sol-gel deposition method were polycrystalline having cubic spinel structure with a small increase in the lattice constant compared to $CoFe_2O_4$. The Raman spectral analyses suggested that the Sc-doped specimens have higher tetrahedral Co^{2+} population than that of pristine $CoFe_2O_4$. The magnetic hysteresis curves of the $Sc_xCoFe_{2-x}O_4$ specimens indicated that the saturation and remanent magnetization decrease proportionally with the increase of Sc composition (x). The decrease in the ferrimagnetic parameters is understandable in terms of the octahedral substitution of non-magnetic Sc^{3+} ions. However, the octahedral Sc^{3+} ions caused an increase of the coercivity.

Keywords : ferrite, scandium, thin film, magnetic properties, structural properties

1. Introduction

Magnetic spinel compounds composed of Fe and some other 3*d* transition-metal ions have attracted incessant research interest for decades due to a wide range of technological applications as well as a variety of magnetic and electronic properties [1]. As a member of the spinel group materials, $CoFe_2O_4$ is a ferrimagnetic insulator [2] in which the magnetic ions occupy either the 8*a* (tetrahedral) or the 16*d* (octahedral) sites surrounded by four and six oxygen anions (O^{2-} at the 32*e* sites), respectively.

The magnetic properties of $CoFe_2O_4$ are significantly affected by the occupation of Co^{2+} ion in either tetrahedral (A) or octahedral (B) sites of the spinel lattice. When $CoFe_2O_4$ is in perfect inverse-spinel configuration, the A sites are occupied by only Fe^{3+} ions with spin magnetic dipole moment of ~5 μ_B, while the B sites are occupied by equal amount of Fe^{3+} and Co^{2+} ions with the magnetic moment of ~5 μ_B and ~3 μ_B, respectively. The anti-parallel spin alignment between A and B sites can explain the ferrimagnetism of $CoFe_2O_4$ below ~790 K [3, 4] due to the net magnetic moment of ~3 μ_B per formula unit, equivalent to magnetization of 380 emu/cm^3 (= 76 emu/g).

On the other hand, experimental studies on $CoFe_2O_4$ have suggested that a portion of the Co^{2+} ions must occupy the A sites. The inversion parameter δ [5] for the ionic configuration $(Co^{2+}_{1-\delta}Fe^{3+}_{\delta})^A[Co^{2+}_{\delta}Fe^{3+}_{2-\delta}]^BO_4$ tends to vary with different synthetic methods [6-9]. The physical and chemical properties of $CoFe_2O_4$ are likely to vary with the value of δ. $CoFe_2O_4$ has shown possible applications including refrigeration, microwave sensing, and biomedicine, recently. For optimizing such potentials, new ferrimagnetic oxides derivable from $CoFe_2O_4$ are worthwhile to be studied. For example, the magnetic properties of the ferrimagnet are variable by replacing Co^{2+} ions by other metallic ions without changing the crystal structure.

The objective of the present study is to investigate the effects of Sc substitution in Fe sites on the structural and magnetic properties of the cobalt ferrites ($CoFe_2O_4 \rightarrow Sc_xCoFe_{2-x}O_4$). Substitution of other metallic elements has been adopted for tailoring the intrinsic properties of the ferrites such as magnetic hysteresis and electromagnetic absorption [2, 4, 10]. Sc atom has one *d* electron ($4s^2$, $3d^1$) in the outer shells so that the ionized Sc in $Sc_xCoFe_{2-x}O_4$ is likely to have no *d* electron, while the Co and Fe ions have a number of *d* electrons. The $Sc_xCoFe_{2-x}O_4$ specimens

*Corresponding author: Tel: +82-32-835-8271
Fax: +82-32-835-0778, e-mail: pjy@inu.ac.kr

were prepared as thin films by sol-gel method. The structural properties of the $Sc_xCoFe_{2-x}O_4$ specimens were investigated by X-ray diffraction (XRD) and Raman spectroscopy. The electronic structure of $Sc_xCoFe_{2-x}O_4$ including ionic valences of Sc, Co and Fe were investigated by X-ray photoelectron spectroscopy (XPS). The magnetic hysteresis curves of the specimens were investigated by vibrating sample magnetometry (VSM).

2. Experimental

A series of scandium-doped cobalt ferrite specimens with compositions $Sc_xCoFe_{2-x}O_4$ were prepared by using a sol-gel deposition method on Si(100) substrates under the following sequence. (1) Preparation of the precursor solution by dissolving $Fe(NO_3)_3{\cdot}9H_2O$, $Co(CH_3CO_2)_2{\cdot}4H_2O$ and $Sc(NO_3)_3{\cdot}xH_2O$ in 2-methoxyethanol (20 ml) and ethanolamine (2 ml) at 110 °C. (2) Repetition of spin-coating the substrate using the precursor solution at 3000 rpm for 20 s followed by pre-heating at 300 °C for 5 min. (3) Post-annealing of the gel film in air at 800 °C for 4 h.

The crystalline structure of the specimens was monitored by using XRD (Cu K_α line, wavelength = 0.15418 nm) in the grazing-incidence geometry with fixed X-ray incidence angle of 4°. The vibrational modes of the specimens were investigated by Raman scattering spectroscopy employing a diode laser (wavelength = 514 nm, power = 1 mW). The XPS measurements on the specimens were performed using Al K_α line (photon energy = 1486.7 eV). The magnetic hysteresis curves of the specimens were measured at room temperature by using VSM in which the external magnetic field applied parallel to the film's plane was varied up to 15 kOe. The specimens contain grains with the size mostly in the 50-150 nm range observed by scanning electron microscopy. The thicknesses of the specimens are in the 250-300 nm range.

3. Results and Discussion

As shown in Fig. 1, the crystal structures of all the $Sc_xCoFe_{2-x}O_4$ specimens were investigated by XRD in comparison with $CoFe_2O_4$. The Sc-doped films are shown to maintain the same crystal structure of $CoFe_2O_4$. The estimated lattice constants (a_o) of the $Sc_xCoFe_{2-x}O_4$ specimens are 0.8377, 0.8384 and 0.8394 nm, respectively, for x = 0.1, 0.2 and 0.3. The value of a_o increases with increasing Sc composition (x) from that of $CoFe_2O_4$ (0.8358 nm) [11], so that a_o for x = 0.3 is larger than that of $CoFe_2O_4$ by 0.4 %. As the Sc composition increased further, secondary phases such as Sc_2O_3 and Co_3O_4 were detected as shown in the XRD pattern of the x = 0.5

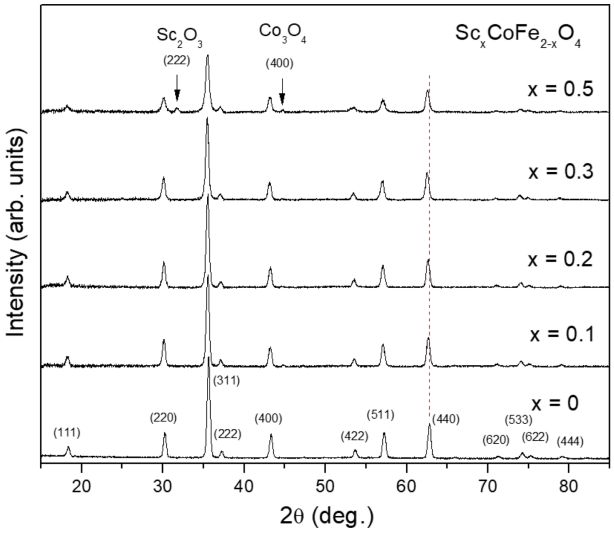

Fig. 1. (Color online) X-ray diffraction patterns of thin-film $Sc_xCoFe_{2-x}O_4$.

specimen. The appearance of the secondary phases implies solubility limit of x < 0.5 for Sc in $Sc_xCoFe_{2-x}O_4$.

In Figs. 2(a), 2(b) and 2(c), 2*p*-photoelectron binding-energy (B-E) spectra for Sc, Fe and Co, respectively, of the $Sc_xCoFe_{2-x}O_4$ specimens obtained by using XPS are exhibited. Firstly, for the Sc 2*p* spectra, two major peaks are observed near 401 and 405 eV. They are ascribed to the spin-orbit (s-o) splitting, $2p_{3/2}$ and $2p_{1/2}$, in Sc^{3+} ion as designated in Fig. 2(a). In Fig. 2(b), the $2p_{3/2}$ and $2p_{1/2}$ peaks for Fe ions are peaked at about 710.5 and 723.9 eV, respectively. The 2*p* s-o energy splitting of 13.4 eV implies that the Fe ions have valence +3. The ionic radius of octahedral Sc^{3+} ion is known to be 0.0745 nm, while that of octahedral high-spin Fe^{3+} ion is 0.0645 nm. The difference in ionic radius between Sc^{3+}(B) and Fe^{3+}(B) is adoptable to explain the increase in a_o with increasing Sc composition as indicated by the XRD analyses. In Fig. 2(c), the $2p_{3/2}$ and $2p_{1/2}$ peaks for Co ions are located at about 779.6 and 795.5 eV, respectively. The Co 2*p* spectra with the s-o splitting of 15.9 eV imply that the Co ions have valence +2.

It is seen that the 2*p*-electron B-E's of Sc^{3+} ion shift to lower energies as the Sc composition increases. For both $2p_{3/2}$ and $2p_{1/2}$ electrons the B-E's of x = 0.3 are smaller by about 0.5 eV compared to those of x = 0.1. On the other hand, the B-E's of Fe^{3+} and Co^{2+} ions remain at the same energies for all the Sc compositions.

Belonging to 3*d* transition-metal group, Sc^{3+} ion differs from Fe^{3+} and Co^{2+} in that it lacks *d* electron in its outermost shell, while Fe^{3+} and Co^{2+} have 5 and 7 *d* electrons, respectively. Thus, the existence of *d* electrons in the upper shell seems to affect the 2*p* photoelectron kinetic

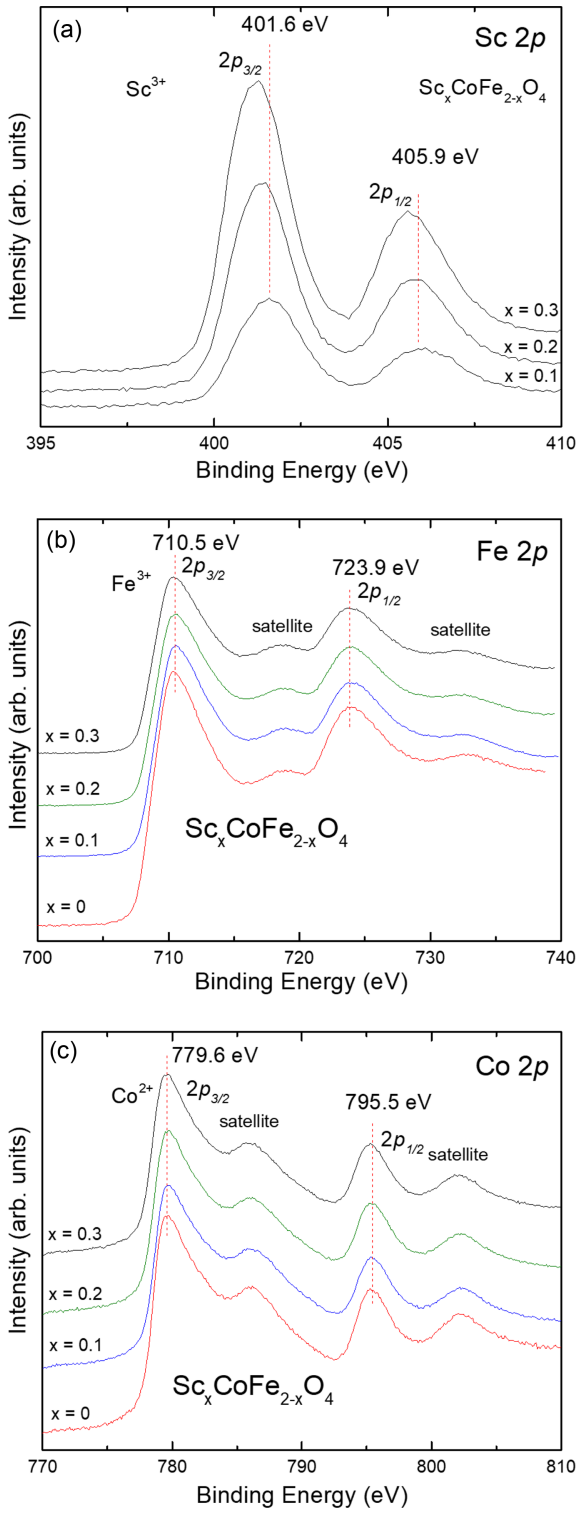

Fig. 2. (Color online) X-ray photoelectron spectra of (a) Sc 2*p*, (b) Fe 2*p* and (c) Co 2*p* electrons of $Sc_xCoFe_{2-x}O_4$ specimens.

energy. The satellites appeared for Fe^{3+} and Co^{2+} 2*p* spectra are attributable to the energy loss of the photoelectrons due to their interaction with the spin-polarized *d* electrons

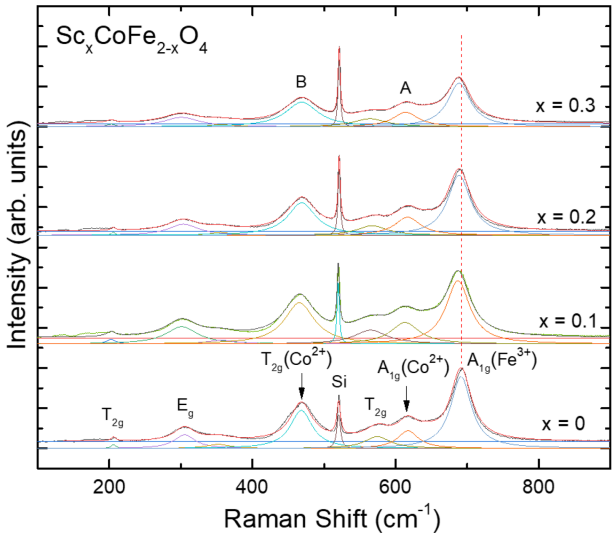

Fig. 3. (Color online) Raman spectra of $Sc_xCoFe_{2-x}O_4$ specimens. Solid curves below the experimental curve represent the result of curve-fitting.

in those ions. The asymmetric shapes of the Fe and Co 2*p*-electron peaks in Figs. 2(b) and 2(c) indicate that the peaks are composed of two origins, e.g., Fe^{3+}(B) and Fe^{3+}(A) at the higher B-E [12].

In Fig. 3, the Raman spectra of the $Sc_xCoFe_{2-x}O_4$ specimens are exhibited in comparison with that of $CoFe_2O_4$ [11]. The Raman spectra of the $Sc_xCoFe_{2-x}O_4$ specimens exhibit similar patterns to that of the $CoFe_2O_4$ specimen. The Raman peaks above 600 cm^{-1} have been explained in terms of A_{1g} vibrational modes for symmetric stretching of O^{2-} ions at the A sites [13]. Thus, the peaks at 693 and 615 cm^{-1} for $CoFe_2O_4$ are assigned to $A_{1g}(Fe^{3+}\text{-}O^{2-})$ and $A_{1g}(Co^{2+}\text{-}O^{2-})$, respectively. The peaks below 600 cm^{-1} for $CoFe_2O_4$ are assigned to T_{2g} (580, 470, 207 cm^{-1}) and E_g (305 cm^{-1}) vibrational modes corresponding to symmetric and anti-symmetric bending of O^{2-} ions at the B sites, respectively [5, 13]. Especially, the 470 cm^{-1} peak is strong for $CoFe_2O_4$ [13, 14], while it is absent for the Raman spectrum of Fe_3O_4 [15]. So, it can be ascribed to T_{2g} mode involving Co^{2+}(B) ions. Thus, the Raman spectra contain peaks ascribed to both tetrahedral (615 cm^{-1}) and octahedral (470 cm^{-1}) Co^{2+} ions [13, 14].

It is noticeable that the A_{1g} peaks near 693 cm^{-1} of the Sc-substituted specimens are located slightly lower energies than that of $CoFe_2O_4$. The low-energy shift for the x = 0.3 specimen is about 5 cm^{-1}. Such low-energy shift of the A_{1g} mode can be understood in terms of the increase of the Fe-O bond length due to the increase of the lattice constant by the Sc substitution in the spinel lattice.

The relative Co^{2+} population at the A and B sites of the

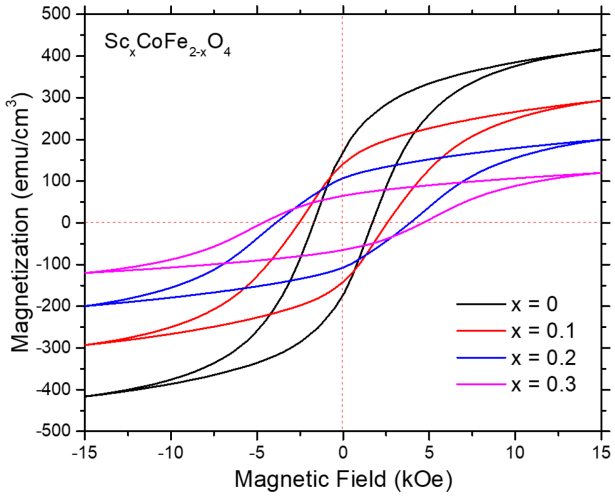

Fig. 4. (Color online) Magnetic hysteresis curves of $Sc_xCoFe_{2-x}O_4$ specimens.

$Sc_xCoFe_{2-x}O_4$ specimens was estimated by curve-fitting the Raman spectra, as shown in Fig. 3, to get the areal ratio between the 615 cm^{-1} (I_A) and 470 cm^{-1} (I_B) peaks. For the $Sc_xCoFe_{2-x}O_4$ specimens the intensity ratio (I_A : I_B) turned out to be 33:67, 34:66 and 32:68 for x = 0.1, 0.2 and 0.3, respectively. Compared to $CoFe_2O_4$ (30:70), the A site occupancy of Co^{2+} ions in $Sc_xCoFe_{2-x}O_4$ is higher than that of $CoFe_2O_4$. It appears that Sc substitution not merely replaces Fe^{3+} in the B sites but also drives Co^{2+} ions to the A sites.

In Fig. 4, the magnetic hysteresis curves of the $Sc_xCoFe_{2-x}O_4$ specimens obtained by using VSM are exhibited in comparison with that of $CoFe_2O_4$ [11]. A magnetic hysteresis curve used to be characterized by saturation magnetization (M_S), remanent magnetization (M_R) and coercivity (H_C). The pristine $CoFe_2O_4$ specimen exhibited M_S, M_R and H_C of 415 emu/cm^3, 170 emu/cm^3 and 1.7 kOe, respectively. The M_S, M_R and H_C values of the film specimen is comparable to those of a nanoparticle specimen [3] with particle size of ~40 nm, 351 emu/cm^3, 140 emu/cm^3 and 0.93 kOe, respectively.

For the Sc-doped specimens, M_S and M_R decrease but H_C increases with increasing Sc composition compared to those of the $CoFe_2O_4$ specimen. The variations of M_S, M_R and H_C with the Sc composition are depicted using circles in Figs. 5(a), 5(b) and 5(c), respectively. In Fig. 5(a), the experimental M_S data (circles) are compared with the result of theoretical estimation (squares) counting on the decrease of the octahedral magnetic moment due to the increase of non-magnetic Sc^{3+} population and the competition of the octahedral and tetrahedral Co^{2+} population predicted by the Raman spectral analyses. The ionic configuration of the Sc-doped specimens can be expressed as $(Co^{2+}_{1-\delta}Fe^{3+}_{\delta})^A[Sc_xCo^{2+}_{\delta}Fe^{3+}_{2-x-\delta}]^BO_4$ in which δ = 0.33, 0.34 and 0.32 for x = 0.1, 0.2 and 0.3, respectively. The rate of decrease of experimental M_S with x turned out to be larger than that of the theoretical estimation. The disorder introduced in spinel ferrites by doping non-magnetic ions is likely to cause local spin canting that causes additional decrease in the magnetization [16, 17].

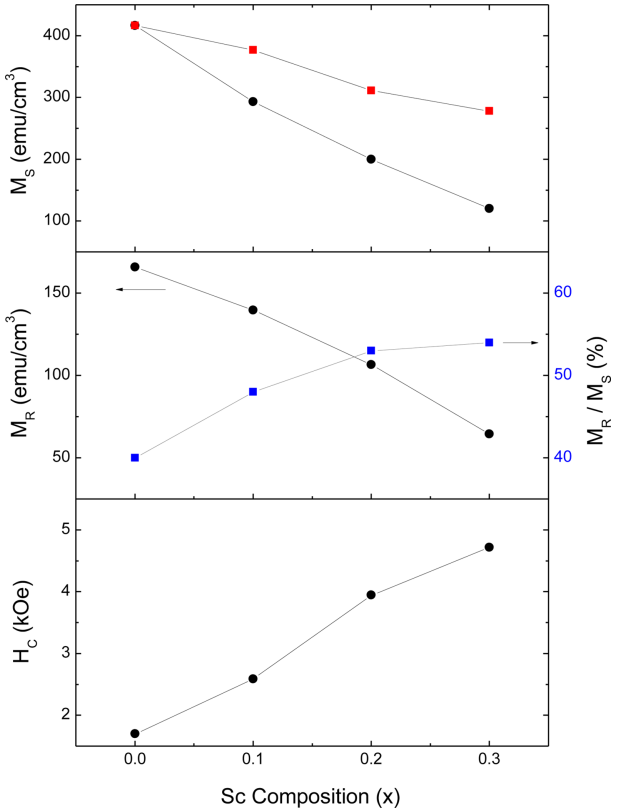

Fig. 5. (Color online) Magnetic parameters of $Sc_xCoFe_{2-x}O_4$ specimens: (a) saturation magnetization (M_S), (b) remanent magnetization (M_R) and (c) coercivity (H_C).

In Fig. 5(b), the squareness ratio (M_R/M_S) is also shown along with the M_R data (circles). As the Sc composition increases, the hysteresis curve becomes more square-like with increasing demagnetization. The squareness ratio approaches to 0.5 with increasing x, implying that the domains were randomly oriented in the demagnetized state [18]. As shown in Fig. 5(c), the value of H_C increases with x, opposite to the behavior of M_S and M_R. The inverse relationship between H_C and M_S can be described using the magnetic anisotropy constant (K) as H_CM_S = (0.96) K, where H_C and M_S have the unit of Oe and G (= $(4\pi)^{-1}$ emu/cm^3), respectively, and K has the unit of J/m^3. The equation was based on a homogeneous rotation coercivity model [18] that was applied to explain the relation between the magnetic parameters for $LiFe_5O_8$ nanocrystallites.

4. Conclusions

The effects of Sc concentration on the physical properties of $Sc_xCoFe_{2-x}O_4$ ferrites have been studied using XRD, Raman spectroscopy, XPS and VSM. Thin-film $Sc_xCoFe_{2-x}O_4$ specimens exhibit spinel structure with the lattice parameter slightly larger (by 0.4 % for x = 0.3) than that of $CoFe_2O_4$. The Raman analyses reveal that the octahedral substitution of Sc^{3+} ions displaces additional (~10 %) Co^{2+} ions from octahedral to tetrahedral sites. The octahedral substitution of non-magnetic Sc^{3+} ions leads to a further decrease in the saturation and remanent magnetization. But the coercivity increases with increasing Sc composition.

Acknowledgment

This work was supported by Incheon National University Research Grant in 2018.

References

[1] G. Herzer, Acta Mater. **61**, 718 (2013).
[2] K. Ugendar, V. Vaithyanathan, L. N. Patro, S. S. R. Inbanathan, and K. K. Bharathi, J. Phys. D: Appl. Phys. **49**, 305001 (2016).
[3] A. Franco and F. C. e Silva, Appl. Phys. Lett. **96**, 172505 (2010).
[4] S. Agrawal, A. Parveen, and A. Azam, J. Magn. Magn. Mater. **414**, 144 (2016).
[5] P. Chandramohan, M. P. Srinivasan, S. Velmurugan, and S. V. Narasimhan, J. Solid State Chem. **184**, 89 (2011).
[6] P. Kumar, S. K. Sharma, M. Knobel, and M. Singh, J. Alloys Comp. **508**, 115 (2010).
[7] A. Thampi, K. Babu, and S. Verma, J. Alloys Comp. **564**, 143 (2013).
[8] R. C. Kambale, P. A. Shaikh, C. H. Bhosale, K. Y. Rajpure, and Y. D. Kolekar, Smart Mater. Struct. **18**, 115028 (2009).
[9] S. Laureti, G. Varvaso, A. M. Testa, D. Fiorani, E. Agostinelli, G. Piccaluga, A. Musinu, A. Ardu, and D. Peddis, Nanotechnology **21**, 315701 (2010).
[10] S. Joshi, M. Kumar, S. Chhoker, A. Kumar, and M. Singh, J. Magn. Magn. Mater. **426**, 252 (2017).
[11] K. J. Kim and J. Park, J. Sol-Gel Sci. Technol. **92**, 40 (2019).
[12] T. Fujii, F. M. F. de Groot, G. A. Sawatzky, F. C. Voogt, T. Hibma, and K. Okada, Phys. Rev. B **59**, 3195 (1999).
[13] V. Georgiadou, V. Tangoulis, I. Arvanitidis, O. Kalogirou, and C. Dendrinou-Samara, J. Phys. Chem. C **119**, 8336 (2015).
[14] D. Sharma and N. Khare, Appl. Phys. Lett. **105**, 32404 (2014).
[15] S. Tiwari, R. J. Choudhary, R. Prakash, and D. M. Phase, J. Phys.: Condens. Matter **19**, 176002 (2007).
[16] W. F. Pong, Y. K. Chang, M. H. Su, P. K. Tseng, H. J. Lin, G. H. Ho, K. L. Tsang, and C. T. Chen, Phys. Rev. B **55**, 11409 (1997).
[17] J. F. Hochepied and M. P. Pileni, J. Appl. Phys. **87**, 2472 (2000).
[18] H. Yang, Z. Wang, L. Song, M. Zhao, J. Wang, and H. Luo, J. Phys. D: Appl. Phys. **29**, 2574 (1996).